

## Real-time advanced sensorless control of axial flux synchronous motor

Amir Yassin Hassan<sup>1</sup>, Essamudin Ali Ebrahim<sup>1</sup>, Saber Mohamed Saleh Salem<sup>2</sup>, Mohamed Elzalik<sup>3</sup>

<sup>1</sup>Department of Power Electronics and Energy Conversion, Electronics Research Institute, Cairo, Egypt

<sup>2</sup>Department of Electrical Engineering, Faculty of Engineering, Fayoum University, Fayoum, Egypt

<sup>3</sup>Department of Process Control Technology, Faculty of Technology and Education, Beni-Suef University, Beni-Suef, Egypt

### Article Info

#### Article history:

Received Nov 12, 2023

Revised Mar 10, 2024

Accepted Mar 29, 2024

#### Keywords:

Direct torque control

Electric vehicles

IRAFSM

Real-time

SLGBRS

Urban dynamometer driving cycle

### ABSTRACT

Interior rotor axial flux permanent magnet synchronous motor (IRAFSM) sensorless control is essential to inject the motor inside the electric vehicles' tire. The proposed straight-line guided by the reference speed (SLGBRS) sensorless space vector pulse width modulation (SVPWM) inverter-direct torque control (DTC) technique for driving the IRAFSM used for electric vehicles (EVs) is evaluated using laboratory emulator setup. A hardware-in-the-loop (HIL) controller and data acquisition are used as a real-time emulation, while the results are compared with MATLAB simulation results. Both simulation and real-time application of the proposed sensorless control for the IRAFSM offer a good speed response. The results of real-time evaluation are identical with the simulation results so, the control is accurate and suitable for practical applications. Urban dynamometer driving cycle (UDDS) for heavy-duty vehicles is used as a driving cycle for simulation and real time evaluation. UDDS is used to ensure the reliability of the proposed control against a wide range of speed changes to be applicable for many applications. The proposed technique allows utilizing the IRAFSM in many applications that requires less contact and reduced sensors like robotics and inside EV's tire with a good reliable control.

This is an open access article under the [CC BY-SA](https://creativecommons.org/licenses/by-sa/4.0/) license.



### Corresponding Author:

Amir Yassin Hassan

Department of Power Electronics and Energy Conversion, Electronics Research Institute

Joseph Tito St, Huckstep, El Nozha, Cairo, Egypt

Email: amir@eri.sci.eg

### NOMENCLATURE

$U_{da}, U_{qa}$	: Stator d-q axis voltages	$T_e$	: Electromagnetic torque
$i_{da}, i_{qa}$	: Stator d-q axis currents	$P$	: Pole -pairs number
$\psi_{qa}, \psi_{da}$	: Flux in d-q axis	$\psi_{sa}$	: Stator windings field flux
$R_{sa}$	: Resistance of stator windings	$i_{sa}$	: Stator current vector
$L_{da}$	: Inductance of the d axis	$T_l$	: Load torque
$L_{qa}$	: Inductance of the q axis	$\omega_r$	: Angular speed of the rotor
$\psi_f$	: Rotor windings field flux	$B$	: The damping factor
$\delta$	: Torque angle	$J$	: IRAFSM inertia
$n$	: The sector from 1 – 6	$\omega_e$	: Angular speed
$\bar{i}_d$ & $\bar{i}_q$	: The reference d-q axis currents	$m$	: Straight-line slope
$\hat{i}_d$ & $\hat{i}_q$	: The estimated d-q axis currents	$\omega_{est}, \omega_d$	: The estimated and demand speed
$f$	: The fixed clock frequency	$e_\omega, e_\psi, e_T$	: Error in speed, flux, and torque respectively

## 1. INTRODUCTION

The electric motor use is ecologically benign and suits for driving electric automobiles since an internal combustion engine fuel emits harmful pollutants [1]. The permanent magnet synchronous AC motor (PMSACM) is the most suitable for driving electric cars because it does not need external excitation of the rotor [2]. The PMSACM with the axial flux configuration is the best for driving electric cars because it can be placed inside the car tire, but this requires that the motor control is of the wireless type [3]–[5]. Direct torque control (DTC) has very fast torque response and the space vector pulse width modulation (SVPWM) method contains low current and torque ripples [6], [7]. DTC is the best for electric vehicles (EVs) because it ensures a smooth and comfortable torque change for the driver and passengers [8]. The straight-line guided by the reference speed (SLGBRS) sensorless evaluator is one of the adaptive reference system model methods that eliminate the problems associated with the sensor speed evaluator by placing the reference speed as a part of the speed estimation system [9]. The real-time emulation is a certificate of validity of the proposed control method in practice. The hardware-in-the-loop (HIL) and oscillators are the main approved devices to measure the extent to which the simulation results and the real-time performance of the motor match the control [10]–[13].

Recent works of sensorless control of synchronous motors with different control types and switching methods applied practical testing in real-time regardless of the applications. However, the proposed method uses SVPWM – DTC control based on the SLGBRS regarding the EV's applications [14]–[25]. The more reduction in direct contact for measurement and reduction of using sensors, the more degree of freedom in applying the control in many applications [9], [26]. This is the main target of the proposed research work to allow easy use of IRAFSM inside the EV's tire and also in robotics. This research also measures the extent to which the simulation matches the laboratory results of the proposed control method, which appears from the results that it gives a real performance with high efficiency. The following sections of this research include the mathematical equations employed, a description of the laboratory equipment used, the results, and the conclusion.

## 2. IRAFSM MODEL AND DTC WITH SVPWM INVERTER

Under the suppositions that the saturation effect, hysteresis-induced losses, eddy currents, and stray losses are omitted, the IRAFSM's dq0 reference frame (1)–(6) are examined. Since there is no prominent pole effect in the investigated IRAFSM,  $L_d = L_q$ , and the following is the back-EMF [27]–[29].

$$U_{da} = R_{sa} i_{da} + \frac{d\psi_{da}}{dt} - P\omega_r \psi_{qa} \quad (1)$$

$$U_{qa} = R_{sa} i_{qa} + \frac{d\psi_{qa}}{dt} + P\omega_r \psi_{da} \quad (2)$$

$$\psi_{da} = L_{da} i_{da} + \psi_f \quad (3)$$

$$\psi_{qa} = L_{qa} i_{qa} \quad (4)$$

$$T_e = \frac{3}{2} P i_{qa} [\psi_f + (L_{da} - L_{qa}) i_{da}] \quad (5)$$

$$T_e = \frac{3}{2} P i_{qa} \psi_f \quad (6)$$

Changes in the torque can be managed by  $i_{qa}$  for  $L_{da} = L_{qa}$ .

Speed adjustments to three phase AC electric motors may be made via DTC in variable-frequency drives. It is possible to approximate the magnetic flux and torque by measuring the machine voltage and current as in (7)–(10) [28], [30], [31].

$$T_e = P i_{sa} \psi_{sa} \quad (7)$$

$$T_e - T_l - B\omega_r = J \frac{d\omega_r}{dt} \quad (8)$$

$$T_e = \frac{3}{2} \frac{P}{L_{da}} i_{qa} \psi_{sa} \psi_f \sin \delta + \frac{3}{4} \frac{L_{da} - L_{qa}}{L_{qa} L_{da}} \psi_{sa}^2 \sin 2\delta \quad (9)$$

For  $L_d = L_q$

$$T_e = \frac{n}{2} \frac{P}{L_{da}} i_{qa} \psi_{sa} \psi_f \sin \delta \quad (10)$$

The dependence of changing angle  $\delta$  on changing electromagnetic torque is evident from this equation. From (3) and (4):

$$\psi_{sa} = \sqrt{(\psi_{qa})^2 + (\psi_{da})^2} \quad (11)$$

The IRAFSM reference flux is calculated using (12) [9].

$$|\psi_s^*| = \sqrt{\psi_f^2 + \left(\frac{2}{3} \frac{T_e^* L_s}{p \psi_f}\right)^2} \quad (12)$$

A strategy of trial and error is used to evaluate the gains of the PI-controller as in (13)-(18) [20].

$$T_e^* = k_p e + k_i \int e dt \quad (13)$$

$$e_\omega = \omega_{ref} - \omega \quad (14)$$

$$U_d = k_p e + k_i \int e dt \quad (15)$$

$$e_\psi = \psi_s^* - \psi_s \quad (16)$$

$$U_q = k_p e + k_i \int e dt \quad (17)$$

$$e_T = T_e^* - T_e \quad (18)$$

PWM waveforms may be made using MATLAB's SVPWM model, a model for calculating switching times, and sector selection [29], [32]. The switching frequency is 20000 Hz, the DC voltage is 250 volts, and the reference speed is 300 rpm. Reference angle and voltages are as in (19)-(21).

$$\begin{bmatrix} u_d \\ u_q \end{bmatrix} = \frac{2}{3} \begin{bmatrix} 1 & -0.5 & -0.5 \\ 0 & \frac{\sqrt{3}}{2} & -\frac{\sqrt{3}}{2} \end{bmatrix} \begin{bmatrix} u_{an} \\ u_{bn} \\ u_{cn} \end{bmatrix} \quad (19)$$

$$u_{ref} = \sqrt{u_d^2 + u_q^2} \quad (20)$$

$$\alpha = \tan^{-1} \left( \frac{u_q}{u_d} \right) \quad (21)$$

Conversion time in any sector is shown in (22)-(24).

$$T_s = \frac{1}{f} \quad (22)$$

$$T_1 = \frac{\sqrt{3} T_s V_{ref}}{V_{dc}} \sin \left( \frac{n}{3} \pi - \alpha \right) \quad (22)$$

$$T_2 = \frac{\sqrt{3} T_s V_{ref}}{V_{dc}} \sin \left( \alpha - \frac{n-1}{3} \pi \right) \quad (23)$$

$$T_0 = T_f - T_1 - T_2 \quad (24)$$

$$0 \leq \alpha \leq 60^\circ$$

### 3. SENSORLESS EVALUATOR FOR SLGBRS

The three parts of the proposed SLGBRS evaluator are the sensorless evaluator, sensorless adjuster, and IRAFSM reference model, as shown in Figure 1. Explanation of the reference model for IRAFSMs is described in (1)-(4). The (1), (3), and (4) are used to derive the (25) for stator voltage in the d-axis.

$$\mathcal{U}_d = R i_d + \frac{d(L i_d + \psi_f)}{dt} - P\omega_r(L i_q) \quad (25)$$

If  $\omega_e = P\omega_r$ , the current can be driven as (26).

$$\frac{di_d}{dt} = -\frac{R}{L} \hat{i}_d + \omega_e \hat{i}_q + \frac{u_d}{L} \quad (26)$$

The stator voltage equation on the q-axis (27) is derived from (2)-(4).

$$\mathcal{U}_q = R_s i_q + \frac{d(L i_q)}{dt} + P\omega_r(L i_d + \psi_f) \quad (27)$$

Once more, by  $\omega_e = P\omega_r$ , the current may be driven as (28).

$$\frac{di_q}{dt} = -\frac{R}{L} \hat{i}_q - \omega_e \hat{i}_d - \frac{\psi_f}{L} \omega_e + \frac{u_q}{L} \quad (28)$$

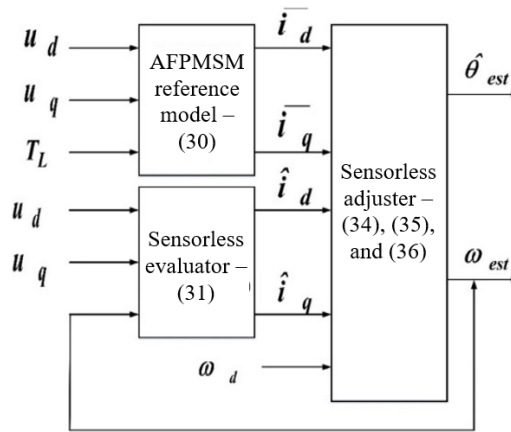


Figure 1. The suggested Straight-line is controlled by a sensorless evaluator of reference speed

Stator current of (26) and (28) for the IRAFSM reference model is recast as the state variable as (29) and (30).

$$\frac{d}{dt} \begin{bmatrix} i_d + \frac{\psi_f}{L} \\ i_q \end{bmatrix} = \begin{bmatrix} \frac{-R}{L} & \omega_e \\ -\omega_e & \frac{-R}{L} \end{bmatrix} \begin{bmatrix} i_d + \frac{\psi_f}{L} \\ i_q \end{bmatrix} + \begin{bmatrix} \frac{u_d}{L} + \frac{R\psi_f}{L^2} \\ \frac{u_q}{L} \end{bmatrix} \quad (29)$$

For  $\bar{i}_d = i_d + \frac{\psi_f}{L}$ ,  $\bar{i}_q = i_q$ ,  $\bar{u}_d = u_d + \frac{R\psi_f}{L}$ , &  $\bar{u}_q = u_q$

$$\therefore \frac{d}{dt} \begin{bmatrix} \bar{i}_d \\ \bar{i}_q \end{bmatrix} = \begin{bmatrix} \frac{-R}{L} & \omega_e \\ -\omega_e & \frac{-R}{L} \end{bmatrix} \begin{bmatrix} \bar{i}_d \\ \bar{i}_q \end{bmatrix} + \frac{1}{L} \begin{bmatrix} \bar{u}_d \\ \bar{u}_q \end{bmatrix} \quad (30)$$

Sensorless evaluator: Substituting the estimated value for the reference value to get (31).

$$\therefore \frac{d}{dt} \begin{bmatrix} \hat{i}_d \\ \hat{i}_q \end{bmatrix} = \begin{bmatrix} \frac{-R}{L} & \hat{\omega}_e \\ -\hat{\omega}_e & \frac{-R}{L} \end{bmatrix} \begin{bmatrix} \hat{i}_d \\ \hat{i}_q \end{bmatrix} + \frac{1}{L} \begin{bmatrix} \hat{u}_d \\ \hat{u}_q \end{bmatrix} \quad (31)$$

Sensorless adjuster: The calculated currents and the reference current differ in the following ways as in (32) and (33).

$$e_d = \bar{i}_d - \hat{i}_d, e_q = \bar{i}_q - \hat{i}_q \quad (32)$$

Subtraction of (30) and (31) yields the difference between reference and estimated currents.

$$\frac{d}{dt} \begin{bmatrix} e_d \\ e_q \end{bmatrix} = \begin{bmatrix} \frac{-R}{L} & \omega_e \\ -\omega_e & \frac{-R}{L} \end{bmatrix} \begin{bmatrix} e_d \\ e_q \end{bmatrix} - (\hat{\omega}_e - \omega_e) \begin{bmatrix} 0 & 1 \\ -1 & 0 \end{bmatrix} \begin{bmatrix} \hat{i}_d \\ \hat{i}_q \end{bmatrix} \quad (33)$$

It is simple to show that the matrix representing the forward channel transfer function is a real, pure positive matrix. The Popov integral inequality may then be solved to get the electrical angular velocity adaptation law utilizing Popov hyper-stability theory [26]. The (34) and the schematic representation in Figure 2 can be used to determine the suggested sensorless speed.

$$\omega_{in} = \{(\hat{i}_q \times \bar{i}_d) - (\hat{i}_d \times \bar{i}_q)\} - \frac{\psi_f}{L}(\bar{i}_q - \hat{i}_q) \quad (34)$$

Where  $\omega_{in}$  is the unadjusted initial estimated speed.

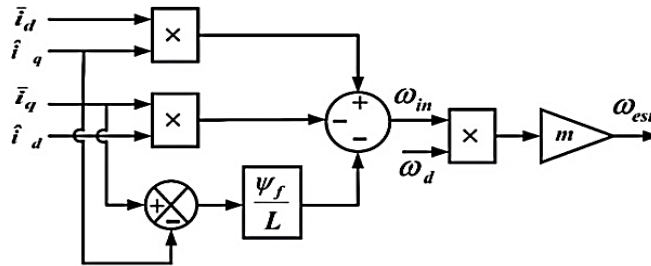


Figure 2. shows the suggested sensorless adjuster in schematic form

The following straight-line (35) is meant to illustrate the connection between evaluated speed and the product of demand speed and initial evaluated speed.

$$\omega_{est} = m \times \omega_{in} \times \omega_d \quad (35)$$

According to the straight-line equation  $\omega_{in} = 10000 \text{ rpm}$  at  $\omega_d = 300 \text{ rpm}$ , the  $m$  is assumed to be 10000, then  $\omega_{est} = 300 \text{ rpm}$ . In order to allow the demand speed sensorless evaluator to traverse a straight path despite changes in the drive's reference speed value, the demand speed setting is used as a judgement parameter. To determine the location of the rotor, the computed speed is integrated as (36).

$$\hat{\theta} = \int_0^t \omega_{est} dt \quad (36)$$

#### 4. SIMULATION VERSUS REAL-TIME RESULTS

In this part, the validity of the suggested approach is demonstrated through the presentation and comparison of real-time emulation results for the test machine with MATLAB/Simulink simulation results. The technology of the real-time digital emulation is very important for the electric motor-drive designing and testing to save money and time and protect the real-physical system. Many test functionalities can be introduced with this technology. This technology is sophisticated in direct converting all MATLAB/Simulink models to run in real-time with the help of an additional software compilation [10].

So, in this paper, the OPAL RT-4510 is used as one of the more efficient real-time simulators in the market. OPAL Company launched it as a two-in-one platform, which means it can function as both a HIL and a fast control prototyping platform. The MATLAB/Simulink programs used in this digital simulator are

compiled using the RT-Lab software suite. Figure 3 presents a schematic diagram for the SLGBRS sensorless control of an IRAFSM inside a vehicle's tire and the real time setup for the controller application.

The entire experimental equipment is shown in Figure 3. It implies the host computer, which includes a console, an OP4510 digital simulator, an OP8660 HIL-controller, and an interface for data gathering. The OP4510-v2 contains a Kintex-7 FPGA and a Xeon 4-core CPU processor for quick real-time emulation. Furthermore, it involves 16 analog channels plus 32-channels for digital input/outputs [11]. The analog output signals are provided through the analog channels via the OP8660 HIL-controller and data acquisition interface to provide supplementary signal conditioning [12]. The values of these output real-time analog signals are limited by the port maximum output voltage (16 V). So, all signals are scaled according to their values. This scaling is done through the model of MATLAB/Simulink. In all cases, the waveforms for the reference and estimated values of torque are scaled by  $\frac{1}{4}$ . In addition, the three-phase stator currents are scaled down 5 times. Furthermore, the reference and estimated speed waveforms are scaled down 35 times to avoid signal saturation at the output ports. Two poles, 11 N.m, and a rated speed of 300 rpm are the IRAFSM characteristics employed in this work [9].

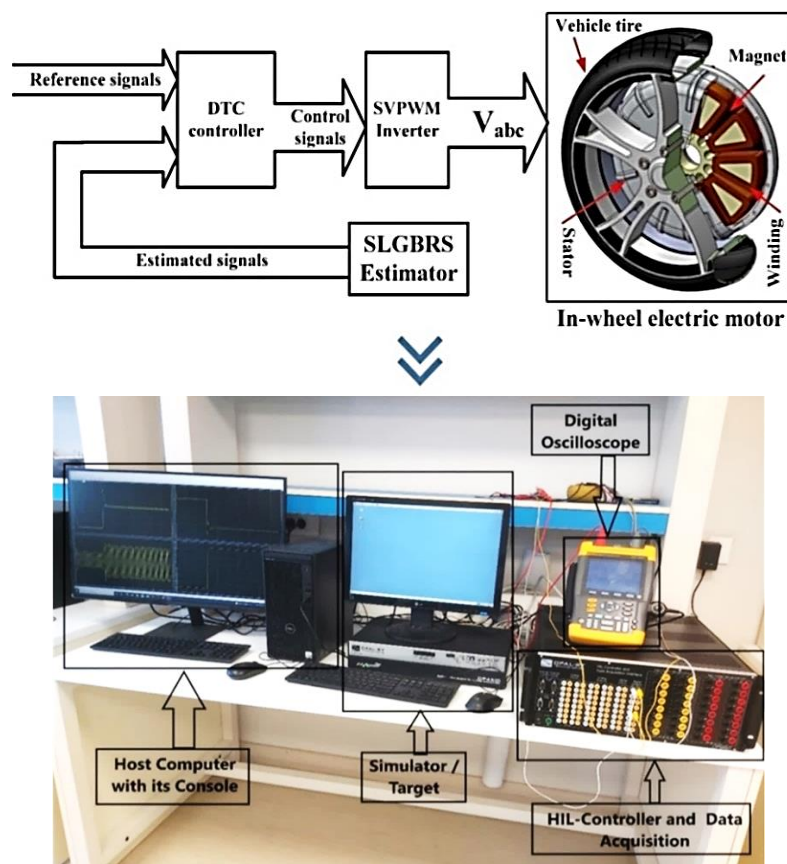


Figure 3. Schematic diagram for the SLGBRS sensorless control and the laboratory setup for the platform of the OPAL-RT real-time digital emulation

Figures 4-9 represent the laboratory real-time and simulation results for speed, torque, and current. It can be observed that they are all quite close. The reference speed trajectory is selected to be aggressive where the reference speed changes from zero to 150 rpm and then from 150 rpm to 225 rpm instantaneously as an impulse change to test the controllability against aggressive changes.

From the speed Figures 4 and 5 for the simulation model and the laboratory measured, the proposed controller response is speed overshoot is about (0.2%), steady-state percentage error is approximately (0.25%), and speed rise time is about (0.05 sec) response to the proposed method. For both the simulation and the lab, the evaluator responded well to the reference torque, as seen in Figures 6 and 7. As seen in Figures 8 and 9, the simulation and laboratory three-phase current signals are extremely similar to sine waves. Table 1 presents the most recent research trends in controlling the IRAFSM [9], [14]-[25]. It is

obvious that the novelty of the proposed research work is that it presents the first study of practical application of sensorless control of IRAFSM with the SLGBRS strategy.

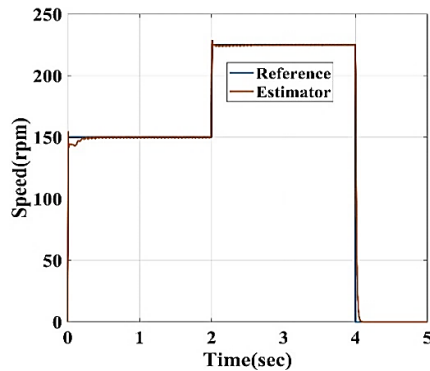


Figure 4. Speed response simulation

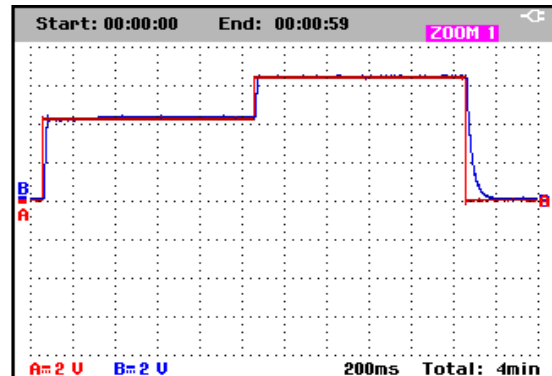


Figure 5. Real-time speed trajectories for reference (Ch. A 2V/div) and estimated (Ch. B 2V/div)

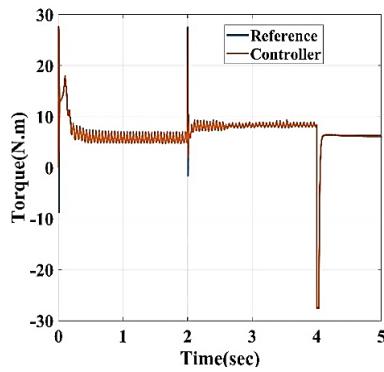


Figure 6. torque response simulation

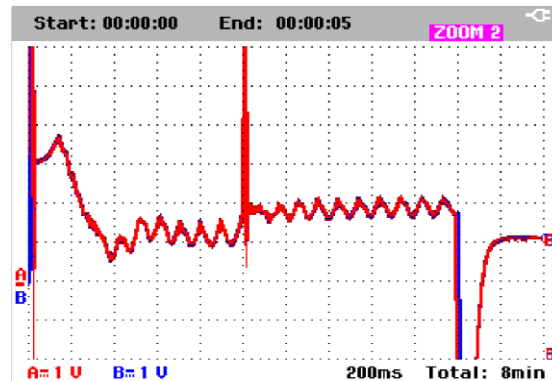


Figure 7. Real-time torque trajectories for reference (Ch. A 1V/div) and estimated (Ch. B 1V/div)

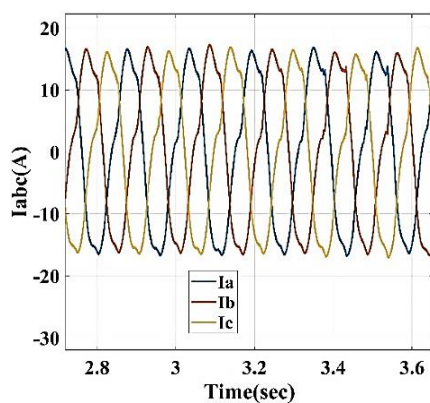


Figure 8. Instantaneous current simulation

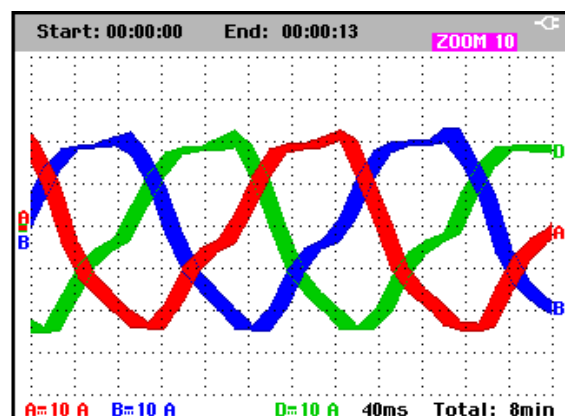


Figure 9. Real-time instantaneous current (Ch. A 10 A/div), (Ch. B 10 A/div), and (Ch. D 10 A/div)

Urban dynamometer driving cycle (UDDS) is a fuel economy dynamometer test required by the Federal Agency for Environmental Protection that simulates the traffic in the city and is used to evaluate

light-duty vehicles. UDDS is also referred to as the U.S. Federal Test Procedure cycle, the Constant Volume Sampler cycle in Sweden, and the Australian Design Rules cycle in Australia. It was initially developed as a benchmark for fossil-fueled cars, but it is now used to estimate the range of a battery-powered car per one charge [33]. In this research work, the UDDS is used as an aggressive trajectory with different speed ranges to test the reliability of the controller with a wide range of changes. Figures 10 and 11 show the simulation and laboratory results against the UDDS as a reference speed.

The common use tire (205/55/R16) with a rim diameter equals 16 inches and a section height equals 55 mm is assumed to be the EV's tire. Thus, the overall diameter of the tire will be  $= (16 \times 2.54) + (5.5 \times 2) = 51.64$  cm.

$$\text{The } \frac{\text{km}}{\text{hr}} = \frac{1000}{2\pi \times 60 \times R_{\text{tire}}} = \frac{1000}{2\pi \times 60 \times 25.82 \times 10^{-2}} = 10.28 \text{ rpm. Gear}_{\text{ratio}} = \frac{\text{motor rated speed}}{\text{max.speed} \left( \frac{\text{km}}{\text{hr}} \right) \times 10.28 \text{ rpm}}$$

Then, for UDDS,  $\text{Gear}_{\text{ratio}} = \frac{300}{1369 \times 10.28} = 0.0213$ . It can be observed that the motor speed follows the reference speed (UDDS) with a good response for both simulation and real time laboratory testing. Also, the simulation and laboratory results have quite identical speed responses.

Table 1. Comparison between the proposed and existing control methods of IRAFSM

Reference	Control type	Switching Method	Control parameters				Response		Practical results
			Speed	Flux	Torque	Overshoot	Steady state error	Rise time	
Proposed	DTC	SVPWM	Controlled	Controlled	Controlled	No	Too small	Very small	Yes
[9]	DTC	SVPWM	Controlled	Controlled	Controlled	No	Too small	Very small	No
[14]	Predictive torque control	Switching Table - 2L VSI	No	Controlled	Controlled	No	Yes	Good	No
[15]	DTC	Hysteresis controller	No	Controlled	Controlled	No	Yes	Good	No
[16]	Speed sensor less fuzzy control using an advanced flux concept	SVPWM	Controlled	No	No	Yes	Yes	Good	No
[17]	Field oriented control	SVPWM	No	No	Controlled		Yes		No
[18]	Internal model current controller	SVPWM	Controlled	No	Controlled	Yes	Yes	Good	Yes
[19]	Deadbeat current prediction vector control	Efficiency optimal torque distribution	Controlled	No	Controlled	No	No	Very high (3.7 Sec)	Yes
[20]	Based on cooperative optimization, sliding mode vector control	SVPWM	Controlled	No	Controlled	Yes	Yes	Very high (6 Sec)	Yes
[21]	Vector control	SVPWM	Controlled	No	No	Yes	No	High	Yes
[22]	Speed sensor-less vector control	SVPWM	Controlled	No	No	No	Yes	High	Yes
	Extended Kalman Filter (EKF)								
[23]	Vector Control	Particle swarm optimization	Controlled	No	controlled	Yes	Yes	Good	No
[24]	Fuzzy control	PWM	Controlled	No	No	No	Yes	High	Yes
[25]	Fuzzy-PID control	Fuzzy	Controlled	No	Controlled	No	Yes	Good	No



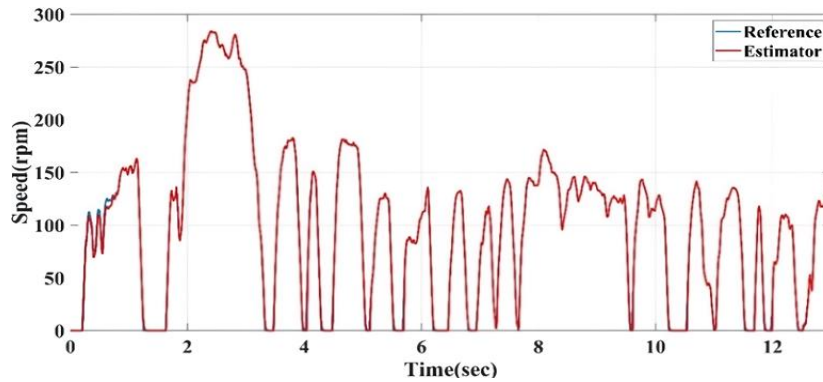


Figure 10. Speed response simulation with UDDS as a reference speed

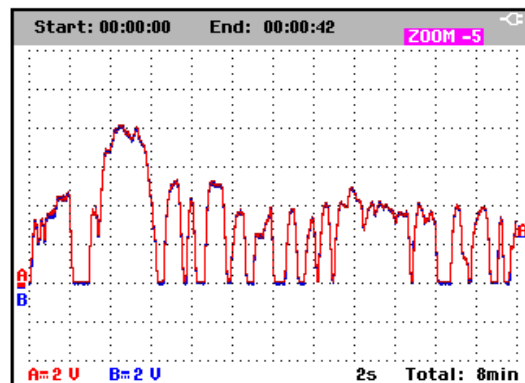


Figure 11. Real-time speed response with UDDS as a reference speed (Ch. A 2 V/div) and estimated (Ch. B 2 V/div)

## 5. CONCLUSION

The aim of this study is to evaluate the IRAFSM sensorless control practically for the purpose of inserting the motor inside the EV's tire. The laboratory results characteristics are like finger print from the MATLAB simulation results so, the real time evaluation proved the accuracy of the suggested control technique. UDDS driving cycle is employed - as a compatible driving cycle with application in EVs - to evaluate the control approach for both real-time and simulation and this subserves identical and accurate response. This control technique is evaluated in laboratory and by MATLAB simulation and looks suitable for practical usage.

According to the results, the regulating variables are extremely manageable with this approach, and the system reaction to the suggested method has a minimal overshoot, a modest steady-state error, and a short rising time. The torque follows the reference torque with minimum ripples and the current is approximately sine wave. The innovation of this work is in the use of a practical approach, which proved its viability and showed how its application makes it simpler to use these motors in many applications, including robots and electric cars.




## REFERENCES

- [1] E. A. Nanaki, *Electrical vehicle for smart cities: trends, challenges, and opportunities*. Denmark: Elsevier, 2021.
- [2] A. Hughes and B. Drury, *Electric motors and drives: undamentals, types and applications*. Oxford: Elsevier, 2019. doi: 10.1016/C2017-0-03226-3.
- [3] S. Wahsh, J. Shazly, and A. Yassin, "Steady state heat conduction problems of AFPMSM using 3D Finite Element," in *2016 Eighteenth International Middle East Power Systems Conference (MEPCON)*, Dec. 2016, pp. 949–953. doi: 10.1109/MEPCON.2016.7837011.
- [4] S. Wahsh, A. Yassin, and J. Shazly, "Effect of rotor speed on the thermal model of AFIR permanent magnet synchronous motor," *International Journal of Renewable Energy Research*, vol. 7, no. 7, pp. 21–25, 2017.
- [5] F. Nishanth, J. Van Verdegheem, and E. L. Severson, "A review of axial flux permanent magnet machine technology," *IEEE Transactions on Industry Applications*, vol. 59, no. 4, pp. 3920–3933, Jul. 2023, doi: 10.1109/TIA.2023.3258933.




- [6] A. Yassin, M. Badr, and S. Wahsh, "Cuckoo search based DTC of PMSM," *International Journal of Power Electronics and Drive Systems (IJPEDS)*, vol. 9, no. 3, pp. 1106–1115, Sep. 2018, doi: 10.11591/ijpeds.v9.i3.pp1106-1115.
- [7] O. M. Arafa, S. A. Wahsh, M. Badr, and A. Yassin, "Grey wolf optimizer algorithm based real time implementation of PIDDTTC and FDTTC of PMSM," *International Journal of Power Electronics and Drive Systems (IJPEDS)*, vol. 11, no. 3, pp. 1640–1652, Sep. 2020, doi: 10.11591/ijpeds.v11.i3.pp1640-1652.
- [8] F. Ben Salem, *Direct torque control strategies of electrical machines*. London: IntechOpen, 2021. doi: 10.5772/intechopen.80103.
- [9] S. M. Saleh and A. Y. Hassan, "Sensorless based SVPWM-DTC of AFPMSM for electric vehicles," *Scientific Reports*, vol. 12, no. 1, p. 9023, May 2022, doi: 10.1038/s41598-022-12825-x.
- [10] C. Dufour, "Highly stable rotating machine models using the state-space-nodal real-time solver," in *2018 IEEE Workshop on Complexity in Engineering (COMPENG)*, Oct. 2018, pp. 1–10. doi: 10.1109/CompEng.2018.8536236.
- [11] B. R. Ravada and N. Reddy Tummuru, "Power management and control of grid connected microgrid with inbuilt EV charging for residential homes," in *2019 IEEE 5th International Conference for Convergence in Technology (I2CT)*, Mar. 2019, pp. 1–5. doi: 10.1109/I2CT45611.2019.9033706.
- [12] I. Abari, M. Hamouda, M. Sleiman, J. B. H. Slama, H. Y. Kanaan, and K. Al-Haddad, "Open-circuit fault detection and isolation method for five-level PUC inverter based on the wavelet packet transform of the radiated magnetic field," *IEEE Transactions on Instrumentation and Measurement*, vol. 71, pp. 1–11, 2022, doi: 10.1109/TIM.2022.3144235.
- [13] A. Y. Hassan, S. A. E.-M. Wahsh, and M. A. E.-L. Badr, "dSP ACE DS 1202 based real time implementation of cuckoo search optimized FDTTC of PMSM," in *2018 Twentieth International Middle East Power Systems Conference (MEPCON)*, Dec. 2018, pp. 1126–1133. doi: 10.1109/MEPCON.2018.8635223.
- [14] A. Malyshev and A. Ivanov, "Direct torque control of the Axial Flux permanent magnet motor," in *2019 Dynamics of Systems, Mechanisms and Machines (Dynamics)*, Nov. 2019, pp. 1–8. doi: 10.1109/Dynamics47113.2019.8944673.
- [15] M.-F. Tsai, T.-C. Lee, C.-S. Tseng, Y.-Y. Chen, and C.-H. Lin, "Modeling and verification of an Axial-Flux permanent magnet motor with cogging torque ripple," in *2013 IEEE International Conference of IEEE Region 10 (TENCON 2013)*, Oct. 2013, pp. 1–4. doi: 10.1109/TENCON.2013.6718915.
- [16] Y. Ren, Z. Q. Zhu, J. E. Green, Y. Li, S. Zhu, and Z. Li, "Improved duty-ratio-based direct torque control for dual three-phase permanent magnet synchronous machine drives," *IEEE Transactions on Industry Applications*, vol. 55, no. 6, pp. 5843–5853, Nov. 2019, doi: 10.1109/TIA.2019.2938468.
- [17] X. Yuan, W. Zhang, X. Liang, L. Hao, and Y. Liang, "Research of control methods for axial field flux-switching permanent magnet machine," in *2018 21st International Conference on Electrical Machines and Systems (ICEMS)*, Oct. 2018, pp. 1218–1222. doi: 10.23919/ICEMS.2018.8549042.
- [18] Y.-S. Choi, H. H. Choi, and J.-W. Jung, "Feedback linearization direct torque control with reduced torque and flux ripples for IPMSM drives," *IEEE Transactions on Power Electronics*, vol. 31, no. 5, pp. 3728–3737, May 2016, doi: 10.1109/TPEL.2015.2460249.
- [19] B. Boazzo and G. Pellegrino, "Model-based direct flux vector control of permanent-magnet synchronous motor drives," *IEEE Transactions on Industry Applications*, vol. 51, no. 4, pp. 3126–3136, Jul. 2015, doi: 10.1109/TIA.2015.2399619.
- [20] J. Zhao, L. Zheng, S. Wang, and M. Hua, "Research on deadbeat current prediction vector control system of axial flux permanent magnet synchronous motor for electric bus based on efficiency optimal torque distribution method," *IEEE Access*, vol. 7, pp. 128384–128393, 2019, doi: 10.1109/ACCESS.2019.2939759.
- [21] J. Zhao, M. Hua, and T. Liu, "Research on a sliding mode vector control system based on collaborative optimization of an axial flux permanent magnet synchronous motor for an electric vehicle," *Energies*, vol. 11, no. 11, p. 3116, Nov. 2018, doi: 10.3390/en11113116.
- [22] J. Zhao, M. Lin, L. Jin, and W. Zhang, "Vector control study of axial field flux-switching permanent magnet machine," in *2014 17th International Conference on Electrical Machines and Systems (ICEMS)*, Oct. 2014, pp. 1091–1095. doi: 10.1109/ICEMS.2014.7013651.
- [23] M. A. Mossa, H. Echeikh, Z. M. Ali, M. Ahmed, S. F. Al-Gahtani, and H. M. Sultan, "Design and modeling of a robust sensorless control system for a linear permanent magnet synchronous motor," *Electronics*, vol. 10, no. 8, p. 966, Apr. 2021, doi: 10.3390/electronics10080966.
- [24] J. Zhao, M. Lin, D. Xu, L. Hao, and W. Zhang, "Vector control of a hybrid axial field flux-switching permanent magnet machine based on particle swarm optimization," *IEEE Transactions on Magnetics*, vol. 51, no. 11, pp. 1–4, Nov. 2015, doi: 10.1109/TMAG.2015.2435156.
- [25] H. Aloui, A. Ben Jridi, N. Chaker, and R. Neji, "Fuzzy control for speed tracking of an electrical vehicle enclosing an axial-flux synchronous motor," in *14th International Conference on Sciences and Techniques of Automatic Control & Computer Engineering - STA'2013*, Dec. 2013, pp. 36–42. doi: 10.1109/STA.2013.6783102.
- [26] N. Quang, N. Quang, and N. Van Lanh, "A sensorless approach for tracking control problem of tubular linear synchronous motor," *International Journal of Electrical and Computer Engineering (IJECE)*, vol. 12, no. 3, pp. 2393–2404, 2022.
- [27] C. Sain, A. Banerjee, and P. K. Biswas, *Control strategies of permanent magnet synchronous motor drive for electric vehicles*. Boca Raton: CRC Press, 2022. doi: 10.1201/9781003189558.
- [28] A. Yassin Hassan, M. Abd El-latif Badr, and S. Abd El-monem Wahsh, "Cuckoo search based real time implementation of direct torque control of PMSM," in *2018 Twentieth International Middle East Power Systems Conference (MEPCON)*, Dec. 2018, pp. 235–241. doi: 10.1109/MEPCON.2018.8635189.
- [29] N. Mohan and S. Raju, *Analysis and control of electric drives: simulations and laboratory implementation*. Wiley, 2021.
- [30] S. M. Saleh and A. S. Farag, "Evaluation of the control strategy performance for isolated variable-speed wind turbine using different wind speed models at different load cases under balanced/unbalanced excitation," *European Journal of Electrical Engineering*, vol. 21, no. 4, pp. 341–353, Oct. 2019, doi: 10.18280/ejee.210401.
- [31] A. Y. Hassan, A. G. Rohieem, and S. M. S. Salem, "Direct torque control of non-salient pole AFPMSMs with SVPWM inverter," *International Journal of Power Electronics and Drive Systems (IJPEDS)*, vol. 13, no. 4, pp. 2014–2023, Dec. 2022, doi: 10.11591/ijpeds.v13.i4.pp2014-2023.
- [32] G. Chen, J. Kang, and J. Zhao, "Numeric analysis and simulation of space vector pulse width modulation," *Advances in Engineering Software*, vol. 65, pp. 60–65, Nov. 2013, doi: 10.1016/j.advengsoft.2013.04.017.
- [33] Y. Xu, L. Jiang, B. Wei, and L. Qiu, "An optimal torque distribution strategy for four-motorized-wheel electric vehicle considering energy conversation," *IEEE Access*, vol. 8, pp. 135975–135988, 2020, doi: 10.1109/ACCESS.2020.3008068.

## BIOGRAPHIES OF AUTHORS






**Amir Yassin Hassan**    received his B.Sc. with excellent grade with honor degree in Electrical Engineering from Fayoum University, Egypt, in June 2010. In 2011, he joined the Electronics Research Institute (ERI) as a researcher assistant at Power Electronics and Energy Conversion Department. He obtained his M.Sc. from Fayoum University at 2014 and he became an assistant researcher in ERI. He received his Ph.D. in Electric Drives from Ain Shams University in January 2019 and he became a researcher in ERI. His major interests are electrical drives, artificial intelligence, renewable energy, thermal modelling and electrical/hybrid vehicles modeling, simulation, and control. He can be contacted at email: amir@eri.sci.eg.






**Essamudin Ali Ebrahim**    is an associate professor at Power Electronics and Energy Conversion Department, Electronics Research Institute (ERI), Cairo, Egypt since 2016. He had B.Sc. in Electrical Engineering from Menofia University, Egypt 1988. Then, he received his M.Sc. and Ph.D. both from Cairo University at 1994 and 2001 respectively. His biography was selected by Marquis Who's Who in 2003 and 2007 respectively and was selected also by Biographical Center of Cambridge University, UK in 2004. In addition, Dr. Ebrahim was awarded the scientific excellence prize for his research activities at ERI in 2015, Egypt. His research interests include high-performance drives, renewable energy, power electronics, AI-control, and power quality. He can be contacted at e-mail: essamudin@yahoo.com or essamudin@eri.sci.eg.



**Saber Mohamed Saleh Salem**    received the M.Sc. and Ph.D. degrees in Digital Protection from Cairo University, Cairo, Egypt, in 2005 and 2009. In 2023, he became a professor of Control of Electrical Machines at Fayoum University, Fayoum, Egypt, while continuing his research. He was active in the field of engineering consultancy at the Engineering Research and Consulting Center at the Faculty of Engineering, Fayoum University. He also has contributions as director of the Disaster and Crisis Management Center at the Faculty of Engineering, Fayoum University. His research interests include digital protection, renewable energy, electronic control of electric machines, and digital signal processing. He can be contacted at email: sms08@fayoum.edu.eg.



**Mohamed Elzalik**    received his B.Sc. with excellent grade with honor degree in Process Control Technology from Faculty of industrial Education, Beni-Suef University, Beni-Suef, Egypt. In 2008, he joined the Faculty of Industrial Education, Beni-Suef University as demonstrator at Process Control Technology. He obtained his M.Sc. from Suez University in 2014 and he became an assistant lecturer in Faculty of Industrial Education. He received his Ph.D. in Power and Electric Machines from Beni-Suef University in August 2019 and he became a lecturer in Process Control Technology from Faculty of Industrial Education, Beni-Suef University. His major interests are electrical drives control, renewable energy, artificial intelligence, modeling, simulation, and process control. He can be contacted at email: mohamed.abdelbar@techedu.bsu.edu.eg.